

Journal of the Geological Society

Sedimentology, clay mineralogy and palaeosols of the Mid-Carnian Pluvial Episode in E Spain: insights into humidity and sea-level variations

Jose F Barrenechea, José López-Gómez & Raúl de la Horra

DOI: <https://doi.org/10.1144/jgs2018-024>

Received 31 January 2018

Revised 4 May 2018

Accepted 12 May 2018

© 2018 The Author(s). Published by The Geological Society of London. All rights reserved. For permissions: <http://www.geolsoc.org.uk/permissions>. Publishing disclaimer: www.geolsoc.org.uk/pub_ethics

To cite this article, please follow the guidance at http://www.geolsoc.org.uk/onlinefirst#cit_journal

Manuscript version: Accepted Manuscript

This is a PDF of an unedited manuscript that has been accepted for publication. The manuscript will undergo copyediting, typesetting and correction before it is published in its final form. Please note that during the production process errors may be discovered which could affect the content, and all legal disclaimers that apply to the journal pertain.

Although reasonable efforts have been made to obtain all necessary permissions from third parties to include their copyrighted content within this article, their full citation and copyright line may not be present in this Accepted Manuscript version. Before using any content from this article, please refer to the Version of Record once published for full citation and copyright details, as permissions may be required.

Sedimentology, clay mineralogy and palaeosols of the Mid-Carnian Pluvial Episode in E Spain: insights into humidity and sea-level variations

JOSÉ F. BARRENECHEA¹; JOSÉ LÓPEZ-GÓMEZ^{2*} & RAÚL DE LA HORRA³

¹*Instituto de Geociencias (CSIC-UCM), Dpto de Mineralogía y Petrología, Facultad de Geología, Universidad Complutense, C/ José Antonio Novais 2, 28040 Madrid, Spain.(barrene@ucm.es)*

²*Instituto de Geociencias (CSIC-UCM, Universidad Complutense, C/ Severo Ochoa 7, 28040 Madrid, Spain.(jlopez@geo.ucm.es)*

³*Departamento de Geodinámica, Estratigrafía, Paleontología, Facultad de Geología, Universidad Complutense, C/ José Antonio Novais 2, 28040 Madrid, Spain.(rhorra@ucm.es)*

Abstract: This study examines rainfall variations of the Mid-Carnian Pluvial Episode (CPE) based on the continental fluvial sedimentology, palaeosol and clay mineralogy records of the Stable Meseta (E Spain). In the formation examined, Manuel Fm or K2 Fm, the CPE is represented by three regressive-transgressive sequences (R-T), or subunits K2.1, K2.2 and K2.3, from base to top. Each subunit broadly consists of a genetic stratigraphic sequence bearing well-developed highstand, lowstand and transgressive system tracts (HST, LST and TST). Hydromorphic features in the palaeosols suggest changes in the activity of both ground and surface waters. The clay mineral assemblage is dominated by illite, with a minor presence of kaolinite and traces of smectite in some samples. After ruling out tectonism in the study area, climate and eustatism emerge as the main allogenic controls in the sedimentary record. Differentiated sedimentary facies and architectural elements in the K2.2 subunit were likely controlled by both a more humid climate and source area, while K2.1 and K2.3 were more related to base-level changes and eustatic control. The presence of more waterlogged pedotypes and of kaolinite and traces of smectite in the clay mineral assemblage of K2.2 also indicates increased humidity. Notwithstanding, our data do not point to intense rainfall periods for the CPE in E Spain.

The Late Triassic period in the Tethys realm was mostly a time of greenhouse conditions dominated by a semi-arid, warm climate, interspersed with brief hot phases (Royer 2006). It may have been the only period of the Phanerozoic without evidence of glacial activity (Preto *et al.* 2010). However, perhaps related to high atmospheric CO₂ values (Retallack 2009), the early Julian to Tuvanian of the

Carnian stage experienced a drastic change in the climate conditions of a large number of basins, represented by a humid episode. This is reflected in their continental and marine sedimentary records indicating abrupt interruption of carbonate platforms developing near the tropics, and the spread of fluvial systems on land occupying vast surfaces (Berra 2012). This humid episode was first described as the Carnian Pluvial Episode (CPE) by Simms & Ruffell (1989, 1990), and later as the Carnian Humid Episode (CHE) by the same authors (Ruffell *et al.* 2016). A few years later, however, a world-wide effect of this humid phase was reported by Gianolla *et al.* (1998). Since then, this episode has been described in many basins (Berra & Jadoul 2002; Hornung & Brandner 2005; Rigo *et al.* 2007; Retallack (2009); Roghi *et al.* 2010; Kozur & Bachmann 2010; Lukeneder *et al.* 2012; Arche and López-Gómez 2014; Ogg 2015; Mader *et al.* 2017, among others).

Evidence of this episode have been recently described both in continental and marine sedimentary records (Preto *et al.* 2012; Dal Corso *et al.* 2015; López-Gómez *et al.* 2017). Furthermore, recent works have shown how this pluvial episode is not reflected by a single episode, but by three or four main episodes in marine (Breda *et al.* 2009; Franz *et al.* 2014), continental records (Arche & López-Gómez 2014; Mader *et al.* 2017), or in both records at the same time (López-Gómez *et al.* 2017). However, the lack of available data related to these episodes has meant that little is known about their significance in the CPE sedimentary record. In an effort to gain insight into palaeoclimate and palaeogeographical conditions, the present study examines palaeosols and their relationship with sedimentary data, and the clay mineralogy of the continental record of these episodes in Central Spain.

Geological and stratigraphic setting

The study area comprises the Triassic of E Spain or eastern Iberian plate. During the Late Triassic, Iberia was an emergent plate surrounded by shallow marine environments and located between latitudes 8° N and 15°N (Perri *et al.* 2013) (Fig. 1a). Over this period, there was substantial plate reorganization as Pangaea started to break up (Ziegler & Stampfli 2001). The consequence was syndepositional extensional tectonics and sea-level oscillations conditioning sedimentation processes across vast areas of the Tethys realm (Gianolla & Jacquin 1998). During humid phases, continental fluxes arose from these elevated areas and punctually accumulated during sea-level falls in subsiding areas, interrupting marine sedimentation (Arche and López-Gómez 2014). This continental accumulation has been related to the CPE by the latter authors and is represented by the Manuel Formation defined by Ortí (1974).

The Manuel Fm defined in SE Spain is the so-called K2 Unit of the Valencia Group, which comprises from base to top, respectively, the five subunits K1 to K5 (Ortí 1974; Ortí *et al.* 2017) (Fig. 2). The age for most of the unit is Julian based on palynological analysis (Arche & López-Gómez 2014) and on the ammonites of its lateral equivalent marine Arenal d'en Castell Unit (López-Gómez *et al.* 2017). Outcrops of the Manuel Fm have been described in the Iberian Ranges, Betic Ranges and the Tabular Cover of the Stable Meseta, a narrow area surrounding the easternmost Variscan Iberian Massif (Fig. 1a, b). Prior studies of this unit in these areas have mostly involved stratigraphic and sedimentologic analyses (e.g. Ortí 1974; Fernández & Dabrio 1978; Solé de Porta & Ortí 1982; Henares *et al.* 2012, among others).

The Manuel Fm lies unconformably on the Palaeozoic basement in areas close to the Iberian Massif, and shows a sharp, erosive contact with its underlying K1 Unit (Fig. 2). This contact has been described as a major unconformity separating two main sequences represented by K1, and units K2 to K5 (Ortí *et al.* 2017). The thickness of the Manuel Fm may vary from 5 m in westernmost areas directly on

the basement, to tens of metres in the main depocenters, outside the westernmost stable areas. Based on stratigraphic and sedimentologic data, the Manuel Fm has been divided into three main subunits: K2.1, K2.2 and K2.3, from base to top respectively (Arche & López-Gómez 2014) (Fig. 2).

To address the CPE in E Spain, Arche and López-Gómez (2014) described 28 sections and 3 boreholes, and recently these same authors added 7 sections to include marine equivalent units in the Balearic Islands (López-Gómez *et al.* 2017). On the basis of these studies, these authors differentiated 5 sectors (Fig. 1b), being the sedimentary record of sector 1 the only one basically of continental origin. In the present work we examine different sections of sector 1, located in the Tabular Cover of the Stable Meseta.

Material and Methods

Mineralogical and palaeosol analyses were conducted in the three differentiated sedimentary subunits of the Manuel Fm, K2.1, K2.2 and K2.3 of the study area. From this sector 1, we selected 5 sections of the 12 previously addressed in sector 1 in Arche & López-Gómez (2014) and López-Gómez *et al.* (2017): Alhambra (AH), Villanueva de la Fuente (VF), Alcaraz (AL), Reolid (RE) and Santiesteban del Puerto (ST) (Figs. 1b, 3). Our sedimentological study of the three subunits and their depositional environments is here based on the latter cited works and on new observations. Palaeosols were described into a field scheme of pedotypes following the criteria of Retallack (1988) and eventually classified according to Mack *et al.* (1993). Palaeosols were identified in the field by the presence of root traces, horizonation, and soil structures. Other field observations include soil colour (Munsell Color 1975), the presence of mottles, Fe-Mn concretions, and the characteristics of horizons with carbonate contents (Machette 1985) and parent materials. Petrographic and mineralogical data were obtained in the laboratory

from thin sections and DRX analyses. Pedotypes were classified using the palaeosol classification system of Mack *et al.* (1993).

Textural characterization and classification of sandstones was performed in a routine petrographic study on thin sections. In addition, 62 samples of red mudstone were collected for the mineralogical study. Bulk mineralogy was determined through X-ray diffraction (XRD) patterns, after grinding and homogenization of the samples to $<53\text{ }\mu\text{m}$. Random-oriented powders were examined in a Siemens Kristalloflex 810 diffractometer using Cu-K α at 30 kV and 40 mA, a step size of 0.03 ($^{\circ}2\theta$), and time per step of 1 s (scan rate of $1.8^{\circ} 2\theta/\text{min}$). Clay mineral composition was determined on oriented aggregates of the $<2\text{ }\mu\text{m}$ fraction obtained by sedimentation from an aqueous suspension onto glass slides. Carbonate cements were removed as recommended by Moore & Reynolds (1989), and in some cases, the oriented aggregates underwent heating and solvation with ethylene glycol. The full-width-half-maximum (FWHM) of the illite 10 Å reflection (so-called illite crystallinity), was measured to determine the intensity of the post-sedimentary processes that affected these samples.

Textural characterization of these mudstones was performed on gold-coated chips of selected samples in a JEOL 6400 scanning electron microscope (SEM) equipped with an energy dispersive spectrometer (EDS).

Results

Sedimentology and sequence stratigraphy

Recent works have described the sedimentology of the Manuel Fm in defined sector 1 of E Iberia (Arche *et al.* 2002; Arche & López-Gómez 2014; López-Gómez *et al.* 2017) (Fig. 1b). The reader is referred to these articles for details on this topic. These studies have detected an eastward increase in the marine sedimentary record, in sectors 2 and 3. Based on these works and new field data, a synthesis of the sedimentary characteristics of the Manuel Fm for sector 1 is

provided in figure 4. This study is based on facies descriptions, their associations and their vertical stacking, constituting different sedimentary or architectural bodies in the three subunits.

Subunit K2.1: This subunit, the smallest of the three, shows an erosive base and maximum thickness of 3.5 m. It is normally represented by three main sedimentary bodies less than 1 m thick (Fig. 4). They represent sandy braided and meandering fluvial systems with laterally associated floodplain sediments with soils development (Fig. 5a). Palaeocurrents basically indicate SE direction.

Subunit K2.2: It shows an erosive base and is the thickest of the three subunits, reaching 11m thick. Three main sedimentary bodies, 1 to 1.7 m in thickness (Fig. 4) are represented in this subunit. Vertical stacking of these bodies may constitute multistorey architectures (Fig. 5b). These sedimentary bodies represent sandy meandering and braided fluvial systems with wide channels and laterally associated floodplain sediments containing plant remains, palaeosols and bioturbation. Limestones are massive or finely laminated, constituting bodies lesser than 0.2m thick, and are related to isolated ponds developed on the floodplains. Palaeocurrents obtained from planar and trough cross-stratification indicate S.SE direction.

Subunit K2.3: This subunit shows an erosive base reaching 6 m in thickness. It is normally represented by three main sedimentary bodies with different lithologies. Fine sediments are related to the upper part of the subunit and represented by marls, gypsum and dolomites with microbial lamination. The upper part of this subunit represents the transition to the K3 Unit, of marine origin. Palaeocurrents can be both uni- and bidirectional. It is interpreted as a change from ephemeral sandy braided fluvial systems to marine coastal shabkhas, similar to examples described in the Cretaceous lower Sego Sandstone, Utah, USA, by Cappelle *et al.* (2016).

These fluvial deposits were recently integrated by López-Gómez *et al.* (2017) within the standard lowstand (LST), transgressive (TST) and highstand (HST) system tracts based on correlation of continental sedimentary processes and their coeval shoreline shifts (Fig. 6).

In sedimentological terms, the K2.1 subunit, as the others, starts with the development of an erosive base and a time gap that followed a HST that is related to the late stage of base-level rise during the latest K1 Fm evolution, generating shoreline regression. This erosive surface, or basal surface of forced regression, would also represent the development of a subaerial surface. The main development of sandy bodies in the three subunits is related to the LST, when aggradation of amalgamated channels took place. These aggradation processes are clearly more prominent in subunit K2.2 when compared to K2.1 and K2.3, as the frequent development of meandering systems would be related to periods of low to moderate rates of base-level rise (Miall 2002), thus implying climatic rather than a eustatic control, which would have mostly controlled discharge and transport capacity. Based on general sedimentological criteria, as are the thickness of the sedimentary structures and development of wider channels, internal erosive surfaces, and presence of hydromorphic palaeosols, subunit K2.2 is related to more permanent flooding processes of the fluvial systems when compared to the other two subunits. According to the criteria of Ashley (1990) and Leclair & Bridge (2001), if mesoforms are typically scaled to the size of the channel in which they formed and water depths can be estimated from the thickness of crossbed sets, the three subunits would be related to small-medium channels and low water discharges.

After reaching a maximum regressive stage, the base level would again rise in subunit K2.3 led to semi-permanent ponds in floodplains, decreasing the erosion capacity of channels and inducing marine deposition on fluvial deposits. Evidence of marine influence within fluvial systems such as tidal features, would indicate

flooding episodes, or accommodation in an excess of sedimentation (Catuneanu 2006). A progressive tendency to drier conditions is shown in the overlying K3 Unit, mostly represented by sabkha deposits (Ortí *et al.* 2017).

Mineralogical analysis

The mineral assemblage of most mudstones analyzed by XRD consists of illite (45 to 89 %), quartz (10 to 45 %), and minor proportions (<of 10 %) of orthoclase, albite and hematite. Other mineral phases present in some samples include calcite, dolomite, gypsum, kaolinite, traces of smectite and irregularly interstratified illite/smectite. The most remarkable differences in the mineralogical composition among Manuel Fm subunits are found in samples from the Alcaraz section (Fig. 7a). The mineral assemblage at the base of the K2.1 subunit is formed by illite, quartz, dolomite, gypsum, orthoclase, albite, hematite and irregularly interstratified illite/smectite (Fig. 7a, b). Samples from the K2.1 and K2.2 subunits contain no gypsum or dolomite, and show in turn a decrease in orthoclase and albite contents (which even disappear in some samples), with a concomitant kaolinite increase (up to 15 %) in the clay fraction (Fig. 7a, c). Orthoclase and albite contents are recovered in the K2.3 subunit, along with kaolinite diminution (< 5 %).

In the Reolid and Alhambra sections, the differences in the mineral association among the K.2 subunits are not so clearly visible. Samples from the Reolid section show lower quartz and higher clay contents than those from the Alhambra section. Relative proportions of quartz increase notably in samples from the top of the K2.3 subunit in both sections. In addition, a reduced number of samples from the Alhambra section contain calcite (5 to 15%), while in the Reolid section, dolomite is the only carbonate mineral identified in a few samples. In most cases, the presence of carbonate (either calcite or dolomite) can be related to the development of palaeosols. The clay mineral association is formed almost

exclusively by illite, although minor amounts of kaolinite and smectite were identified in some samples. Kaolinite is a minor constituent (up to 5 %) of the clay mineral assemblage in samples from the K2.1 and K2.2 subunits in the Reolid section and top of K2.1, in the Alhambra section. Traces of smectite (< 5 %) appear in the middle part of the K2.2 subunit and in the K2.1 subunit in both sections.

Our SEM study reveals mudstones dominated by randomly-oriented illite flakes and platy particles, of sizes ranging between 1 and 48 μm , and all intermediate sizes present (Fig. 7d). Chemical compositions determined on clay sized particles and large detrital platy crystals are similar, and can be represented by the structural formula $\text{K}_{1.01}(\text{Mg}_{0.75}\text{Fe}_{1.05}\text{Al}^{\text{VI}}_{2.70})(\text{Al}^{\text{IV}}_{0.72}\text{Si}_{7.28})\text{O}_{20}(\text{OH})_4$.

In samples from the Alcaraz section, gypsum aggregates are found among the illite particles (Fig. 7e). Kaolinite was found as small (2-4 μm) pseudo-hexagonal particles that grow on the walls of partially altered orthoclase crystals forming booklets of hexagonal crystals (Fig. 7f, g), while smectite was only detected as tiny fibres at the margins of some illite particles.

The illite crystallinity data (average FWHM = 0.73, 0.89 and 1.03° $\Delta 2\theta$ in the Alhambra, Reolid and Alcaraz sections, respectively) suggest that sedimentary rocks from Alhambra and Reolid sections were subjected to conditions close to the limit between shallow and deep diagenesis, while those from Alcaraz reached the shallow diagenesis realm.

Palaeosols

Palaeosols were mainly developed on muddy and silty wide floodplains both proximally and distally to active channels. Up to 6 pedotypes (P1–P6) were differentiated and classified (Figs. 8, 9). Pedotypes 1, 2 and 3 are found in the lower parts of the stratigraphic logs. Pedotypes 4, 5 and 6 occur laterally related to channelized facies in the K2.2 subunit (Fig. 8). Pedotype 1 developed on clayey

materials that could present nodular gypsum. This pedotype is characterized by poor horizonation, a red colour, fine to medium angular blocky peds, and isolated root traces >1.5 m long. We have classified this pedotype as a Protosol (Fig. 8). Isolated and deeply penetrating roots or *sinkers* are typical of seasonally dry soils where roots need to reach deep groundwater (Retallack 1997). These long roots present a light greenish grey halo around a greenish black carbonaceous core 2–13 cm thick (Fig. 9A). As this weakly developed pedotype shows no other gley features, drab haloed roots traces are interpreted as produced via the reduction of iron around the original fossil root during the burial of the soil (Retallack, 2001). Pedotype 2 presents a red horizon with fine angular blocky peds on top of light red siltstones with common coarse greenish mottles and carbonaceous root traces. Mottling is more abundant towards the base of the profiles (Fig. 9B) suggesting gleying caused by activity of ground waters for some time of the year (Krauss & Aslan 1999). The poor development of this pedotype classifies it as a Gleyed Protosol (Fig. 8). Pedotype 3 is characterized by a subsurface horizon formed by coalescing coarse mottles of light greenish grey with common carbonaceous roots traces not exceeding 60 cm in length penetrating a red clayey horizon with secondary gypsum nodules (Fig. 9C). The continuous greenish level on top of the profiles suggests gleization caused by surface waters or perched water tables (Krauss & Aslan 1999) and it is classified as a Gleysol (Fig. 8). A purple hue characterizes the subsurface horizon of Pedotype 4 (Fig. 9D). This horizon features thin platy peds and a gradual contact with the underlying horizon, which is light red and often has greenish 1–5 cm thick mottles. When the subsurface horizon is bluish green, the underlying horizon is usually purplish red and shows few but coarse greenish mottles. Iron-manganese nodules are conspicuous in some of the profiles. The features of this pedotype are probably related to waterlogged soils due to the presence of stagnant water ponds for some part of the year (Fitzpatrick 1983; Retallack 1997) and it is classified as a Gleysol (Fig. 8). Finally, Pedotypes 5 and 6 (Figs. 9E and 9F) are calcareous palaeosols with their calcic

horizons showing stage II to III carbonate accumulation (Machette 1985). The calcic horizon in both cases is shallow, in many cases indicative of dry climates (Retallack 2001). However, hydromorphic features such as gley horizons and scarce mottling are also present as in Gleyed Calcisols (Fig. 8). Probably, those soils started its development in distal and elevated locations from the active channels that provided good conditions for the precipitation of pedogenic carbonates. Later, as the accommodation space increased, those soils were buried under new material and located in low areas of the floodbasin. There, the soils were poorly drained or submerged under the water table explaining the gley features on top of a calcic horizon (Krauss & Aslan 1999).

Discussion

The sector 1 examined here is basically represented by a continental record, however, the coastal and marine environments described in the nearby sector 2 conditioned the development of fluvial systems in sector 1. In addition, rivers in sector 1 were also controlled by a combination of climate shifts and source area activity, that is, upstream controls, as described by Holbrook & Shumm (1998), which also conditioned erosion, fine sediment sources and soil development. In general, fluvial responses to changes in sediment load and discharge are mainly climate related, while responses to base-level shifts are mainly related to tectonism and eustatic fluctuations (Catuneau 2006). Tectonism, or the third main allogenic control is not considered here, as sector 1 is included in the so-called Tabular Cover or Stable Meseta (Fig. 1b), a narrow promontory of Variscan rocks east of the Iberian Massif that remained stable during the Mesozoic (Arche & López-Gómez 2014).

The relationship between main sea-level oscillations and sedimentary processes, clay characteristics, and palaeosol development across the three subunits is shown

in figure 6. These three subunits broadly represent three genetic stratigraphic sequences, and the whole sedimentary record constitutes three regressive-transgressive sequences (R-T) in the Manuel Fm. Influence of sea-level oscillations was also reported from mid-Carnian equivalent units in the Alps and Central European basin (Franz et al., 2014; Gattolin et al., 2014).

The palaeosols of subunits K2.1 and K2.2 display hydromorphic features formed under the effects of groundwater, surface-water, or both. The long root traces of pedotype P1, located at the lower part of the K2.1 subunit, suggest deep water tables. However, this situation changes at the top of the subunit, where the activity of ground waters and surface waters is evidenced by the presence of pedotypes P2 and P3, reflecting waterlogged conditions of the floodplain for some part of the year (Krauss & Aslan 1999). The lower part of subunit K2.2 is characterized by the presence of pedotype P4 showing purple to blue Bw horizons bearing Fe-Mg nodules. More persistent stagnant waters were probably related to the gleying of this soil type, implying that more flood water was transported into the floodplain during the sedimentation of the lower part of the K2.2 subunit. The appearance of the carbonate pedotypes P5 and P6 at the top of this subunit in all the sections examined is related to a change to drier climate conditions, which is later evidenced by the sabkha deposits of the K3 Unit.

The presence of hydromorphic features in a soil reflects local waterlogging for some months of the year rather than regional palaeoclimate conditions (Krauss & Aslan 1999; Retallack 2001). However, a general upwards trend from pedotype 1 to pedotype 6 is observed in all the sections. Pedotypes P2, P3, and P4 are associated with a period of wetter conditions than during the development of pedotypes P1, P5, and P6. Topographically, low, poorly-drained areas could provide suitable gleization conditions, but the amount of water required was probably supplied by seasonal rains and floods. The trend towards drier conditions indicated by the presence of evaporites in subunit K2.3 is in agreement with the

development of pedotypes P6 at the top of the K2.2 subunit. The presence of pedogenic carbonate is usually related to dry and seasonal climates and absent from soils developed under humid climates (Retallack 2001). Some authors suggest that soils receiving less than 760 mm yr⁻¹ would have discrete carbonate horizons (as in Pedotypes E and F), and that around 1000–1200 mm yr⁻¹ carbonate is washed down from the profile (Retallack 2001; Alonso-Zarza 2003). Stiles et al. (2001) related mean annual precipitation ranging from 850 to 1500 mm yr⁻¹ with modern soils with common Fe-Mn nodules. Probably, during the development of pedotype P4, rich in Fe-Mn nodules, the precipitation reached a minimum of 1200 mm yr⁻¹.

One of the objectives of this study is to relate changes in the mineralogical composition with palaeoclimatic conditions. Clay minerals are frequently used as palaeoclimate indicators, as they can be considered the result of weathering and soil formation processes (Chamley 1989). However, many other factors may affect these processes such as the parent materials, the topography, or the time available for them to proceed, which in turn depends on tectonic and geomorphologic stability (Velde 1995; Meunier 2005). According to Chamley (1989), only sites that are tectonically stable over long periods of time are suitable for recording climate changes. As discussed above, our study area was rather stable tectonically and thus its clay mineralogy will likely reflect, to some extent, the combined record of source rock and climate. Also, though the original clay mineral association may be masked by diagenetic reactions, illite crystallinity data reflect that samples from the Alcaraz section were affected by shallow diagenesis, and might therefore have preserved, at least partially, the primitive clay mineral assemblage. However, samples from the Reolid and Alhambra sections will probably be more influenced by diagenetic transformations.

The mineral assemblage in the mudstones analyzed in the Alcaraz section evidence a noteworthy change among the Manuel Fm subunits (Fig. 7a). The

presence of gypsum and dolomite at the base of K2.1 subunit can be related to arid conditions during deposition. Nevertheless, samples from the K2.1 and K2.2 subunits contain no dolomite and only traces of gypsum, and they are characterized by the presence of kaolinite along with a significant decrease in orthoclase and albite. The SEM study suggests kaolinite formation at the expense of orthoclase dissolution (Fig. 7f, g). This in turn reflects increased chemical weathering, and thus a change to more humid conditions, rather than a diagenetic transformation, which would have likely produced kaolinitization of any sample with feldspar. Kaolinite has been extensively described in weathering and soil profiles developed under intense rainfall and warm climates (Chamley 1989; Meunier 2005). Deepthy & Balakrishnan (2005) examined the clay mineral assemblages formed in tropical regions receiving low and high rainfall and concluded that kaolinite (together with Al-Fe oxides) was the dominant clay mineral in the latter, while kaolinite and smectite appeared in the former. Therefore, the mineralogical changes described in subunits K2.1 and K2.2 likely result from increased chemical weathering, though not too intense, because otherwise kaolinite and smectite would be the dominant clay minerals instead of illite. In fact, the presence of aggregates of tiny gypsum crystals (Fig. 7 e) recognised during the SEM study in these samples (not detected on XRD analyses) suggests periods of higher evaporation. The relative decrease in kaolinite and the concomitant increase in orthoclase and albite in the K2.3 subunit (Fig. 7a) could be interpreted as a return to less humid conditions.

On the other hand, the presence of illite as the dominant clay mineral most probably results from the size degradation of detrital micas during weathering of the source area that eventually would be incorporated into the sediments as clay particles through illuviation. The textural relationships observed in our SEM study seem to corroborate this hypothesis, since large detrital mica plates and illitic clay particles show a similar composition, and a wide range of intermediate sizes was

observed (Fig. 7d). Accordingly, combined mechanical and chemical weathering processes were probably responsible for the observed changes in the clay mineral associations.

Clay mineralogy of the Alhambra and Reolid sections was largely dominated by illite, with minor amounts of kaolinite and traces of smectite in a few samples (Fig. 6), from K2.2 and to a lesser extent from the K2.1 subunit, suggesting relatively increased rainfall conditions during their deposition, which is in agreement with above discussed results from the Alcaraz section. The scarcity of kaolinite and smectite supports our idea that chemical alteration was not too intense, as would be expected under a warm, humid tropical climate.

Once tectonism control was ruled out, fluvial responses to base-level shifts during the Manuel Fm sedimentation indicate more developed maximum regressive conditions and a lesser transgressive pulse in subunit K2.2 when compared to K2.1 and K2.3. Further, changes in sediment load and sediment discharge and the characteristics shown by the soils and clays also point to a more humid climate for subunit K2.2 or middle of the CPE sedimentary record, when compared to subunits K2.1 and K2.3. Notwithstanding, these data on their own do not suggest high rainfall rates for the CPE in E Spain, only when compared to other generally drier Late Triassic episodes.

Conclusions

As in other areas of the Peri-Tethys realm, the continental record of the CPE in the Stable Meseta, E Spain, or Manuel Fm, is represented by three main regressive-transgressive sequences (R-T) and its whole sedimentary record is constituted by subunits K2.1, K2.2 and K2.3 from base to top respectively. Each subunit is broadly represented by a genetic stratigraphic sequence with well-developed HST, LST and TST. They mainly consist of fining-upwards sequences related to braided

and meandering fluvial systems with palaeosols developing in fine sediments related to floodplains. Once tectonism in the study area is discarded, climate and eustatism emerge as the main allogenic controls in the sedimentary record. Sedimentological, palaeosol and mineralogical analyses are the basis to studying climate variations in the Manuel Fm. Differentiated sedimentary facies and architectural elements point to more base-level change and eustatic controls on subunits K2.1 and K2.3, while the K2.2 subunit was more related to climate and source area control. The presence of larger channels and thicker refill sequences with plants remains in this latter subunit also indicates more water in the fluvial systems. These data fit in well with the P2, P3 and P4 pedotypes and kaolinite identified in subunit K2.2, also indicating more humidity in this subunit. In any case, none of these data indicate substantial rainfall episodes for the CPE in E Spain, and only stand out if compared to other generally drier Late Triassic episodes.

Acknowledgements

This work was supported by project CGL2014-52699P. Critical comments by Mathias Franz, Jacopo Dal Corso and anonymous reviewer clearly improved the manuscript. A. Arche is thanked for creative suggestions and discussion on the subject. The authors thank the staff of the ICTS-CNME in Madrid (Spain).

References

- Alonso-Zarza, A. M. 2003. Palaeoenvironmental significance of palustrine carbonates and calcretes in the geological record. *Earth-Science Reviews* **60**, 261–298. [https://doi.org/10.1016/S0012-8252\(02\)00106-X](https://doi.org/10.1016/S0012-8252(02)00106-X)
- Arche, A. & López-Gómez, J. 2014. The Carnian Pluvial Event in Western Europe: new data from Iberia and correlation with the Western Neotethys and Eastern North America – NW Africa regions. *Earth-Science Reviews*, **128**, 196–231. <http://dx.doi.org/10.1016/j.earscirev.2013.10.012>

Ashley G.M. 1990. Classification of large-scale subaqueous bedforms: a new look to an old problem. *Journal of Sedimentary Petrology*, **60**, 160-172.

Bennett, C. E., Kearsy, T. I. *et al.* 2016. Early Mississippian sandy siltstones preserve rare vertebrate fossils in seasonal flooding episodes. *Sedimentology*, **63**, 1677–1700, doi: 10.1111/sed.12280

Berra, F. 2012. Sea-level fall, carbonate production, rainy days: How do they relate? Insight from Triassic carbonate platforms (Western Tethys, Southern Alps, Italy). *Geology*, **40** (3), 271–274. doi: 10.1130/G32803.1

Berra, F. & Jadoul, F. 2002. Evidence of a "Mid-Carnian" transgression in the Western Southern Alps (Lombardy Italy): stratigraphic and paleogeographic implications. *Rivista Italiana di paleontologia e stratigrafia*, **108** (1), 119–131.

Breda, A., Preto, N. *et al.* 2009. The Carnian Pluvial Event in the Tofane area (Cortina d'Ampezzo, Dolomites, Italy). *Geo Alp*, **6**, 80–115.

Cappelle, M. V., Stukins, S. *et al.* 2016. Fluvial to tidal transition in proximal, mixed tide-influenced and wave-influenced deltaic deposits: Cretaceous lower Sego Sandstone, Utah, USA. *Sedimentology*, **63**, 1333–1361, doi: 10.1111/sed.12267

Catuneanu, O. 2006. *Principles of Sequence Stratigraphy*. Elsevier. Oxford, 375p.

Chamley, H. 1989. *Clay Sedimentology*. Springer-Verlag. Berlin Heidelberg. 623 p.

Dal Corso, J., Mietto, P. *et al.* 2012. Discovery of a major negative ^{13}C spike in the Carnian (Late Triassic) linked to the eruption of Wrangelia flood basalts. *Geology*, **40**, 79–82. DOI10.1130/G32473.1

Dal Corso, J., Gianolla, P. *et al.* 2015. Carbon isotope records reveal synchronicity between carbon cycle perturbation and the "Carnian Pluvial Event" in the Tethys realm (Late Triassic). *Global and Planetary Change*, **127**, 79–90. <https://doi.org/10.1016/j.gloplacha.2015.01.013>

Deepthy, R. & Balakrishnan, S. 2005. Climatic control on clay mineral formation: Evidence from weathering profiles developed on either side of the Western Ghats. *Journal of Earth System Science*, **114-5**, 545–556, <https://doi.org/10.1007/BF02702030>

Díaz-Martínez, E. 2000. Análisis composicional de la Formación Areniscas de Manuel (Triásico Superior) en las secciones de Almansa, Montealegre y Manuel

(provincias de Albacete y Valencia), zona Prebética Oriental: resultados preliminares. *Geogaceta*, **27**, 55–58. ISSN:0213683X

Fernández, J. & Dabrio, C. J. 1978. Análisis sedimentológico de una capa de areniscas (Triásico del borde SE de la Meseta Ibérica). *Estudios Geológicos*, **34**, 475–482.

Fitzpatrick, E. A. 1983. *Soils: Their Formation, Classification and Distribution*. Longman, New York, 353.

Franz, M. & Nowak, K. *et al.* 2014. Eustatic control on epicontinental basins: The example of the Stuttgart Formation in the Central European Basin (Middle Keuper, Late Triassic). *Global and Planetary Change*, **122**, 305–329. <https://doi.org/10.1016/j.gloplacha.2014.07.010>

Gattolin, G., Preto, N. *et al.* 2015. Sequence stratigraphy after the demise of a high-relief carbonate platform (Carnian of the Dolomites): Sea-level and climate disentangled. *Palaeogeography, Palaeoclimatology, Palaeoecology*, **423**, 1–17. [10.1016/j.palaeo.2015.01.017](https://doi.org/10.1016/j.palaeo.2015.01.017)

Gianolla, P. & Jacquin, T. 1998. Triassic sequences stratigraphic framework of western European basins. In: De Gracinsky, P-C., Hardenbol, J., Jacquin, T. & Vail, P. (eds.) *Mesozoic and Cenozoic Sequence Stratigraphy of European Basins*. Society for Sedimentary Geology, Special Publication, **60**, 643–650. ISBN 1-56576-043-3

Gianolla, P., Ragazzi, E. & Roghi, G., 1998. Upper Triassic amber from the dolomites (northern Italy). A paleoclimatic indicator? *Revista Italiana di Paleontologia e Estratigrafia*, **104** (3), 381–389.

Gibling, M. R. 2006. Width and thickness of fluvial channel bodies and valleys fill in the geological record: a literature compilation and classification. *Journal of Sedimentary Research*, **76**, 731–770. DOI: 10.2110/jsr.2006.060

Henares, S., Viseras, C. & Cultrone, G. 2012. Evaluación petrofísica de areniscas fluviales. El ejemplo del Triásico en el sector de Alcaraz (Albacete). *Geogaceta*, **52**, 89–92. ISSN 2173-6545

Holbrook, J. M. & Shumm, S. A. 1998. Geomorphic and sedimentary response of rivers to tectonic deformation: a brief review and critique of a tool for recognizing subtle epeirogenic deformation in modern and ancient settings. *Tectonophysics*, **305**, 287–306. [https://doi.org/10.1016/S0040-1951\(99\)00011-6](https://doi.org/10.1016/S0040-1951(99)00011-6)

Kozur, H. W. & Bachmann, G. H. 2010. The middle Carnian Wet Intermezzo of the Stuttgart Formation (Schilfsandstein), Germanic Basin. *Paleogeography Paleoclimatology Paleoecology*, **290**, 107–119. doi: [10.1016/j.palaeo.2009.11.004](https://doi.org/10.1016/j.palaeo.2009.11.004)

Kraus, M. & Aslan, A. 1999. Palaeosol Sequences in Floodplain Environments: A Hierarchical Approach. *International Association of Sedimentologists Special Publication*, **27**, 303–321. DOI: 10.1002/9781444304190.ch12.

Leclair, S. F. & Bridge, J. S. 2001. Quantitative interpretation of sedimentary structures formed by river dunes. *Journal of Sedimentary Research*, **71**, 713–716.

López-Gómez, J., Escudero-Mozo, M.J. *et al.* 2017. Western Tethys continental-marine responses to the Carnian Humid Episode: Palaeoclimatic and palaeogeographic implications. *Global and Planetary Change*, **148**, 79–95. <http://dx.doi.org/10.1016/j.glopacha.2016.11.016>

Lukeneder, S., Lukeneder, A. *et al.* 2012. Delayed carbonate factory breakdown during the Tethyan-wide Carnian Pluvial Episode along the Cimmerian terranes (Taurus, Turkey). *Facies*, **58** (2), 279–296. DOI 10.1007/s10347-011-0279-8

Machette, M. N. 1985. Calcic soils of the southwestern United States. In: Weide, D.L. (ed) *Soils and Quaternary Geology of the Southwestern United States*. Special Paper of the Geological Society of America, **203**, 10–21.

Mack, G. H., James, W.C. & Monger, H. C. 1993. Classification of paleosols. *Geological Society of America Bulletin*, **105**, 129–136. DOI: [https://doi.org/10.1130/0016-7606\(1993\)105<0129:COP>2.3.CO;2](https://doi.org/10.1130/0016-7606(1993)105<0129:COP>2.3.CO;2)

Mader, N. K., Redfern, J. & Ouataoui, M. 2016. Sedimentology of the Essaouira Basin (Meskala Field) in context of regional sediment distribution patterns during upper Triassic pluvial events. *Journal of African Earth Sciences*, **130**, 293–318, <http://dx.doi.org/10.1016/j.jafrearsci.2017.02.012>

Miall, A. D. 2002. Architecture and sequence stratigraphy of Pleistocene fluvial systems in the Malay Basin based on seismic time-slice analysis. *American Association of Petroleum Geologists Bulletin*, **86** (7), 1201–1216. DOI: <https://doi.org/10.1306/61EEDC56-173E-11D7-8645000102C1865D>

Meunier, A. 2005. *Springer-Verlag*. Berlin Heidelberg. 472 p

Mueller, S., Krystyn, L. & Krüschner, M. 2016. Climate variability during the Carnian Pluvial Phase-A quantitative palynological study of the Carnian sedimentary succession at Lunz am See, Northern Calcareous Alps, Austria.

Paleogeography Paleoclimatology Paleoecology, **441**, 189–211. doi.10.1016/j.palaeo.2015.06.008

Munsell Color (1975). *Munsell soil color charts*. Baltimore, Maryland, Munsell Color, 24.

Ogg, J. 2015. The Mysterious Mid-Carnian "Wet Intermezzo" Global Event. *Journal of Earth Science*, **26** (2), 181–191. DOI: 10.1007/s12583-015-0527-x

Ortí, F. 1974. El Keuper del Levante español. *Estudios Geológicos*, **30**, 7–46.

Ortí, F., Pérez-López, A. & Salvany, J. M. 2017. Triassic evaporites of Iberia: Sedimentological and palaeogeographical implications for the western Neotethys evolution during the Middle Triassic-Earliest Jurassic. *Palaeogeography, Palaeoclimatology, Palaeoecology*, **471**, 157–180, <http://dx.doi.org/10.1016/j.palaeo.2017.01.025>

Perri, F., Critelli, S. *et al.* 2013. Triassic redbeds in the Malaguide Complex (Betic Cordillea-Spain): Petrography, geochemistry and geodynamic implications. *Earth-Science Review*, **117**, 1–28. <https://doi.org/10.1016/j.earscirev.2012.11.002>

Preto, N., Kustatscher, E. & Wignall, P. 2010. Triassic climates-State of art. *Paleogeography Paleoclimatology Paleoecology*, **290**, 1–10. doi: [10.1016/j.palaeo.2010.03.015](https://doi.org/10.1016/j.palaeo.2010.03.015)

Preto, N., Willems, H. *et al.* 2012. Onset of significant pelagic carbonate accumulation after the Carnian Pluvial Event (CPE) in the western Tethys. *Facies*, **60** (2), 719–720. [10.1007/s10347-012-0338-9](https://doi.org/10.1007/s10347-012-0338-9)

Retallack, G. J. 1988. Field recognition of paleosols. *In*: Reinhardt, J. & Sigleo W.R. (eds). *Paleosols and Applications*. Geological Society of America Special Paper, **216**, 1–21.

Retallack, G. J. 1997. *A Colour Guide to Paleosols*. John Wiley & Sons, Chichester, 175.

Retallack, G. J. 2001. *Soils of the Past*. Blackwell. Oxford, 404.

Retallack, G. J. 2009. Greenhouse crisis of the past 300 million years. *Geological Society America Bulletin*, **121**, 1441–1455. doi: [10.1130/B26341.1](https://doi.org/10.1130/B26341.1)

Rigo, M., Preto, N. *et al.* 2007. A rise in the Carbonate Compensation Depth of Western Tethys in the Carnian (Late Triassic): Deep-water evidence for the Carnian Pluvial Event. *Paleogeography Paleoclimatology Paleoecology*, **246**, 188–205. doi: [10.1016/j.palaeo.2006.09.013](https://doi.org/10.1016/j.palaeo.2006.09.013)

Roghi, G., Gianolla, P. *et al.* 2010. Palynological correlation of Carnian humid pulses throughout the western Tethys. *Paleogeography Paleoclimatology Paleoecology*, **290**, 89–106. doi: [10.1016/j.palaeo.2009.11.006](https://doi.org/10.1016/j.palaeo.2009.11.006)

Royer, D. L., Berner, R. A. *et al.* 2004. CO₂ as the primary driver of Phanerozoic climate. *GSA Today*, **14**, 1–10. doi: [10.1130/1052-5173\(2004\)014<4:CAAPDO>2.0.CO;2](https://doi.org/10.1130/1052-5173(2004)014<4:CAAPDO>2.0.CO;2)

Ruffell, A., Simms, M. J. & Wignall, P. B. 2016. The Carnian Humid Episode of the Late Triassic: a review. *Geological Magazine*, **153**, 271–284. <https://doi.org/10.1017/S0016756815000424>

Simms, M. J. & Ruffle, A. H. 1989. Synchronicity of climatic change and extinctions in the Late Triassic. *Geology*, **17**, 265–268. doi: [10.1130/0091-7613\(1989\)017<0265:SOCCAE>2.3.CO;2](https://doi.org/10.1130/0091-7613(1989)017<0265:SOCCAE>2.3.CO;2)

Simms, M. J. & Ruffle, A. H. 1990. Climate and biologic change in the Late Triassic. *Journal Geological Society London*, **147**, 321–327. doi: [10.1144/gsjgs.147.2.0321](https://doi.org/10.1144/gsjgs.147.2.0321)

Soil Survey Staff 1999. *Keys to Soil Taxonomy*. Pocahontas Press, Blackburg, 600.

Solé de Porta, N. & Ortí, F. 1982. Primeros datos cronostratigráficos de las series evaporíticas del Triásico Superior de Valencia (España). *Acta Geológica Hispánica*, **17**, 185–191. ISSN 0567-7505

Stiles, C.A., Mora, C.I., Driese, S.G., 2001. Pedogenic iron-manganese nodules in Vertisols: a new proxy for paleoprecipitation? *Geology* 29, 943–946. doi: [10.1130/0091-7613](https://doi.org/10.1130/0091-7613)

Sun, X. L., Wignall, P. B. *et al.* 2016. Climate warming, euxinia and carbon isotope perturbations during the Carnian (Triassic) crisis in South China. *Earth and Planetary Science Letters*, **444**, 88–100. <https://doi.org/10.1016/j.epsl.2016.03.037>

Velde, B. 1995. *Origin and Minerology of Clays*. Springer-Verlag, Berlin Heidelberg, 334 p

Xu, G., Hannah, J.L. *et al.* 2014. Cause of Upper Triassic climate crisis revealed by Re-Os geochemistry of Boreal black shales. *Paleogeography Paleoclimatology Paleoecology*, **395**, 222–232. <https://doi.org/10.1016/j.palaeo.2013.12.027>

Ziegler, P.A. 1988. *Post-Hercynian plate reorganization in the Tethys and the Artic-North Atlantic domains*. Developments in Geotectonics, Elsevier, 22B, 711–756. Amsterdam.

Ziegler, P.A. & Stampfli G.M. 2001. Late Paleozoic-Early Mesozoic plate boundary reorganization: collapse of the Variscan Orogen and opening on the Neotethys. *Natura Bresciana, Museo Civico di Scienze, Annales*, **25**, 17–34.

LEGENDS TO FIGURES

Fig. 1. (a) Palaeogeographic framework of the Iberian plate (IB) during the Late Triassic (modified from López-Gómez *et al.* 2017), and present-day geographical location of the study area. **(b)** These four sectors and sections (black points) have been examined in our prior work. The sections examined here are (red triangles): AH Alhambra, AL Alcaraz, RE Reolid, ST Santiesteban del Puerto, and VF Villanueva de la Fuente.

Fig. 2. The Manuel Fm (K2 Unit) and its three subunits (K2.1, K2.2, K2.3). These subunits are here shown in two of the studied sections (Alhambra and Reolid). K1 to K5 constitute the Valencia Group (Ortí 1974).

Fig. 3. The five sections of the Manuel Fm examined and their subunits. All these sections belong to Sector 1 (see Fig 1b).

Fig. 4. Differentiated facies, facies associations, their vertical stacking and sedimentological interpretations in the Manuel Fm.

Fig. 5. (a) Trough and planar cross-stratification and a fining-upward trend in the multistorey fluvial system of subunit K2.1 in the Alhambra section. Bar for scale 1.2 m. **(b)** Superimposed fining-upward sequences in subunit K2.2 in Santiesteban del Puerto. **(c)** Grey marls (arrow 1) and white carbonaceous fine sandstones and limestone layers (arrow 2) thinner than 15 cm developing into the massive red mudstones of subunit K2.3 in the Reolid section. Bar for scale 1.6 m.

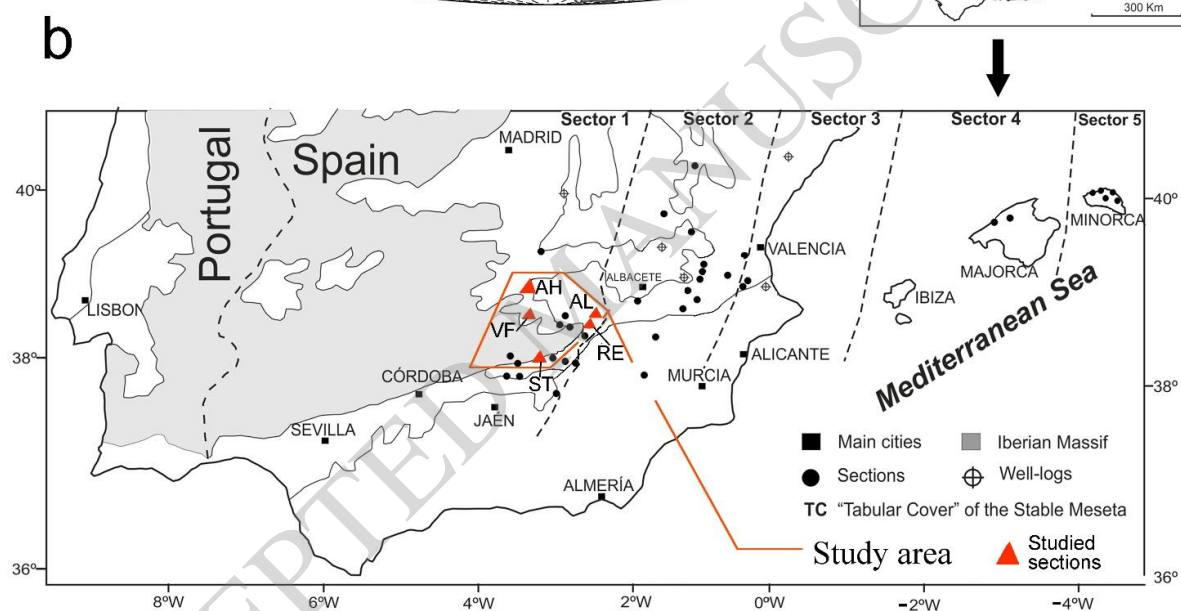
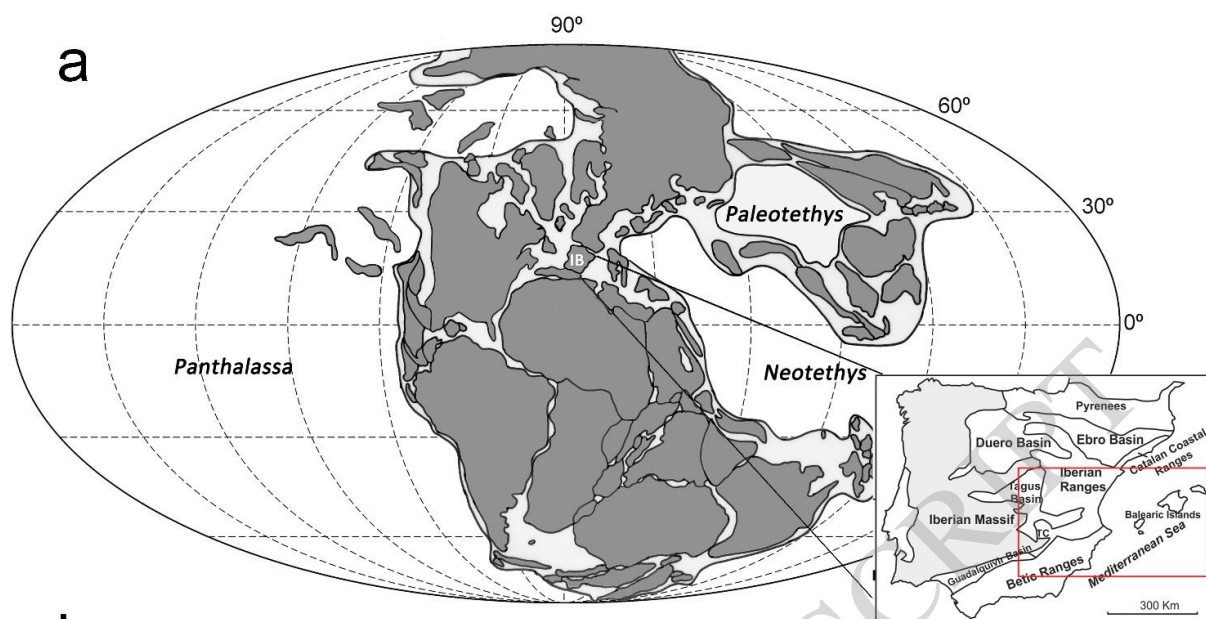
Fig. 6. Standard section of the Manuel Fm showing main continental-coastal line changes. Regressive-transgressive sequences (R–T), lowstand systems tract (LST), transgressive systems tract (TST) and highstand systems tract (HST) with the mineralogy and palaeosols main characteristics.

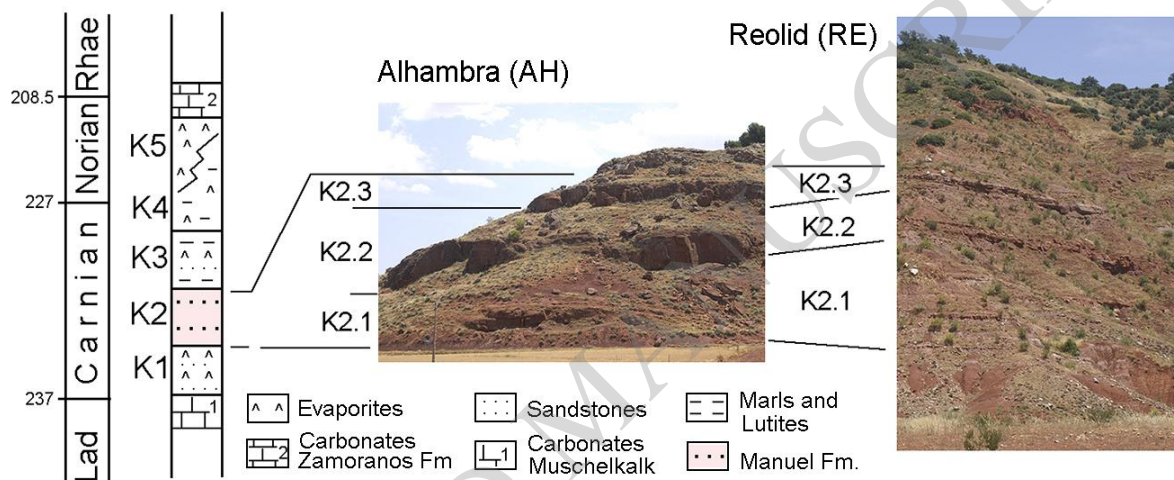
Fig. 7. a) Mineralogical composition determined from XRD patterns of samples collected along the Alcaraz section. **b)** XRD patterns of random-oriented powder (black) and oriented aggregate (red) of a sample under the base of K2.1 subunit and **c)** of a sample from subunit K2.2. **d)** SEM image of illites showing a wide

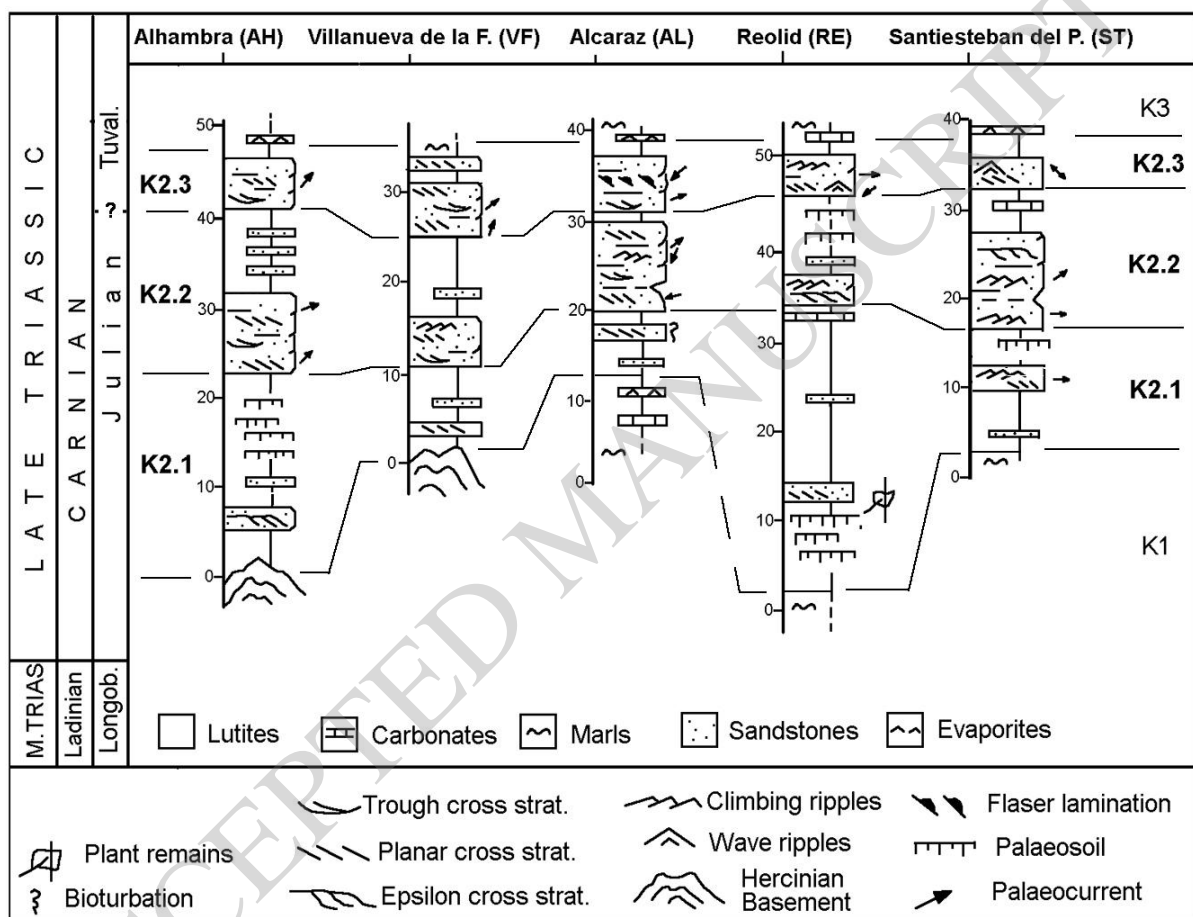
range of particle sizes (0.5 to 10 μm) in a sample from the Alhambra section, **e)** Aggregate of gypsum crystals in a sample from the Alcaraz section. **f)** Hexagonal booklets of kaolinite crystals on the walls of a partially corroded orthoclase crystal in a sample of the K2.2 subunit in the Alcaraz section. Enclosed area enlarged in **g)** Closer view of the kaolinite hexagonal crystals. Gy: gypsum; Illi: illite; Kaol: kaolinite; Or: orthoclase; Ab: albite; Dol: dolomite; Q: quartz; Hem: hematite.

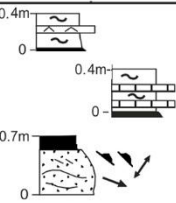
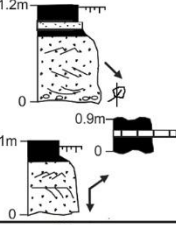
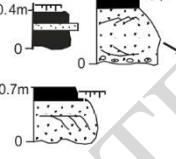
Fig. 8: General stratigraphic section showing a fining upwards tendency from pedotype P1 to P6. Representative profiles of the pedotypes are also included. USDA Soil Taxonomy system (Soil Survey Staff 1999) was used for identification of the horizons.

Fig. 9: A) Field picture of the weakly developed P1 pedotype. The top of the profile is marked by a subtle change in soil structure and the beginning of the “sinker” root trace (white arrow). B) Sequence of the P2 profiles. These profiles form a compound sequence: the rate of pedogenesis exceeds the rate of sedimentation (eg. Krauss & Aslan 1999). Note the downward increase in mottling from the top of the profiles (white triangles) suggesting groundwater activity. C) On the contrary, the P3 pedotype is characterized by a downward decrease in gley mottles as produced by surface water. The profiles in the picture, however, were later affected by the water table (marked with dotted black line). D) The P4 pedotype shows a bluish green top horizon and Fe-Mn nodules due to perched water tables, but also other features as mottling probably due to groundwater activity. E) The shallow calcic horizon of pedotype P5 reaches stage II of carbonate accumulation (Machette 1985). However, gleying is evidenced by the overlying greenish horizon. Note how gley features decrease downwards such as in the presence of surface waters. F) The layer consisting of coalescing nodules of the P6 pedotype characterizes soils as more mature than the P5 palaeosols. Those profiles were located in higher areas away from the channels and flooding activity during their development and probably under arid or semiarid climatic conditions. However, once buried, they were also affected by surface water as suggested by their Bg horizons. Shorthand for labelling horizons follows Retallack (1988).







Unit	Subunit	Facies	Vertical stacking (Facies Assoc.)	Environment	
Manuel Formation	K-2.3	1, 2, 4, 5, 7, 12, 13 15, 18, 19 20, 21, 22 23		Ephemeral braided sandy river deposits with isolated small aeolian dunes drawn by marine transgressive deposits where supratidal evaporites in mudflats developed.	1- Planar cross-stratification. 2- Trough cross-stratification. 3- Epsilon cross bedding. 4- Current ripples. 5- Oscillation ripples. 6- Overturned lamination. 7- Erosive surface. 8- Fossil trunk or trunk remains. 9- Convolute lamination. 10- Planar surface with high-iron content. 11- Parallel lamination. 12- Bioturbation. 13- Soil developments. 14- Plant remains. 15- Climbing ripples. 16- Massive mudstones. 17- Trace fossils. 18- Massive limestones (cm scale) 19- Marls with diffuse lamination. 20- Microbial lamination. 21- Flaser lamination. 22- Evaporite molds. 23- Isolated aeolian dunes.
	K-2.2	1, 2, 3, 4 6, 7, 8, 9, 11, 12, 13 14, 15, 16, 17, 24		Sandy braided deposits with shallow, wide channels with irregular flashy discharge and periods of full-bank flows. Trunk remains. Active channels of meandering fluvial systems and avulsion with overbank deposits development and small ponds with development of carbonatic deposits.	
	K-2.1	1, 2, 3 4, 7, 10, 11, 12, 13, 15		Sandy braided and meandering fluvial systems. Periods of low-water level indicating marked seasonality and avulsion processes with overbank deposits.	

